11. Guthoff RF, Zhivov A, Stachs O. In vivo confocal microscopy, an inner vision of the cornea – a major review. Clin Experiment Ophthalmol 2009;37:100-17.
12. Martone G, Casprini F, Traaversi C, Lepri F, Picherri P, Caporossi A. Pseudoexfoliation syndrome: in vivo confocal microscopy analysis. Clin Experiment Ophthalmol 2007;35:582-5.
13. Sbeity Z, Palmiero PM, Tello C. Liebmann JM, Ritch R. Non-contact in vivo confocal scanning laser microscopy in exfoliation syndrome, exfoliation syndrome suspect and normal eyes. Acta Ophthalmologica 2009;Oct 23.
14. Hu Y, Matsumoto Y, Adan ES, et al. Corneal in vivo confocal scanning laser microscopy in patients with atopic keratoconjunctivitis. Ophthalmology 2008;115:2004-12.
15. Quadrado MJ, Popper M, Morgado AM, Murta JN, Best JAV. Diabetes and corneal cell densities in humans by in vivo confocal microscopy. Cornea 2006;25:761-68.
16. Mocan MC, Durukan I, Irkec M, Orhan M. Morphologic alterations of both the stromal and subbasal nerves in the corneas of patients with diabetes. Cornea 2006;25:769-73.
17. SchlÖtzer-Schrehardt U, Koca M, Naumann GOH, Volkholz H. Pseudoexfoliation syndrome: ocular manifestation of a systemic disorder? Arch Ophthalmol 1992;110:1752-56.
18. Thorleifsson G, Magnusson KP, Sulem P, et al. Common sequence variants in the LOXL1 gene confer susceptibility to exfoliation glaucoma. Science 2007;317:1397-400.
19. Wang L, Yamasita R, Hommura S. Corneal endothelial changes and aqueous flare intensity in pseudoexfoliation syndrome. Ophthalmologica 1999;213:318-91.
20. Miyake K, Matsuda M, Inaba M. Corneal endothelial changes in pseudoexfoliation syndrome. Am J Ophthamol 1989;108:49-52.

21. Streeten BW, Gibson SA, Dark AJ. Pseudoexfoliative material contains an elastic microfibillar-associated glycoprotein. Trans Am Ophthalmol Soc 1986;84:304-20.

Figure legends

Figure 1. Corneal epithelial and endothelial cell densities of eyes with the pseudoexfoliation (PEX) syndrome, their clinically unaffected fellow eyes, and eyes of normal control subjects. Statistical significance is denoted by: $^{**}P<0.01$, $^{*}P<0.05$.

Figure 2. Cellular densities of anterior, intermediate and posterior stroma of eyes with the pseudoexfoliation (PEX) syndrome, their clinically unaffected fellow eyes, and eyes of normal control subjects. Statistical significance is denoted by: $^{**}P<0.01$, $^{*}P<0.05$.

Figure 3. Subbasal long nerve fiber density (LNFD) and nerve branch density (NBD) in eyes with the pseudoexfoliation (PEX) syndrome, their clinically unaffected fellow eyes, and eyes of normal control subjects. Statistical significance is denoted by: $^{**}P<0.01$.

Figure 4. In vivo confocal microscopic images of the subbasal nerve plexus in patients with pseudoexfoliation (PEX) syndrome and a normal control subject.

A. Representative image from a normal control subject showing subbasal nerve plexus with long nerve fibers running parallel to Bowman layer. The nerve fibers appeared to be straight with minimal tortuosity. The subbasal long nerve fiber density (LNFD) was 31.3 nerves/mm^2 and the nerve tortuosity was grade 1.

B. Representative image from a PEX eye showing very tortuous nerves with significant convolutions throughout their course. The tortuosity grade was 4. Also, note the intensive infiltration of dendritic cells (arrows) in close vicinity of nerve fibers.

C. Confocal image of the subbasal nerve plexus of another PEX eye showing the thinning of the nerves, short nerve sprouts, fewer branches from the main nerve trunk, and significantly

decreased nerve density. The LNFD was 6.3 nerves/mm^2. Arrows indicate dendritic cell infiltration.

D. Confocal image of a PEX fellow eye, showing moderately tortuous subbasal nerve plexus with a tortuosity grade of 3 and LNFD of 18.8.

Figure 5. Confocal microscopic images showing exfoliation material (XFM) in the subbasal nerve plexus layer of a patient with pseudoexfoliation (PEX) syndrome.

A. Nerve fiber thinning with tortuous morphology can be seen (arrowhead), and XFM (arrows) are seen in close vicinity of the pathogenic nerve fibers.

B. Hyperreflective deposits (arrows) indicative of XFM can be seen in the subbasal amorphous layer of the cornea from another patient in the PEX eye group.

Figure 6. Representative confocal microscopic images of the endothelial layers of pseudoexfoliation (PEX) syndrome eye, PEX fellow eye, and normal control eye group. **A.** Normal subject with regularly arranged hexagonal endothelial cells.

B. PEX eye showing increase in pleomorphism and polymegethism and decrease in cell density. Intense hyperreflective materials indicative of exfoliation material (XFM) can be seen.

C. PEX fellow eye showing similar changes of endothelial cells and deposition of XFM.

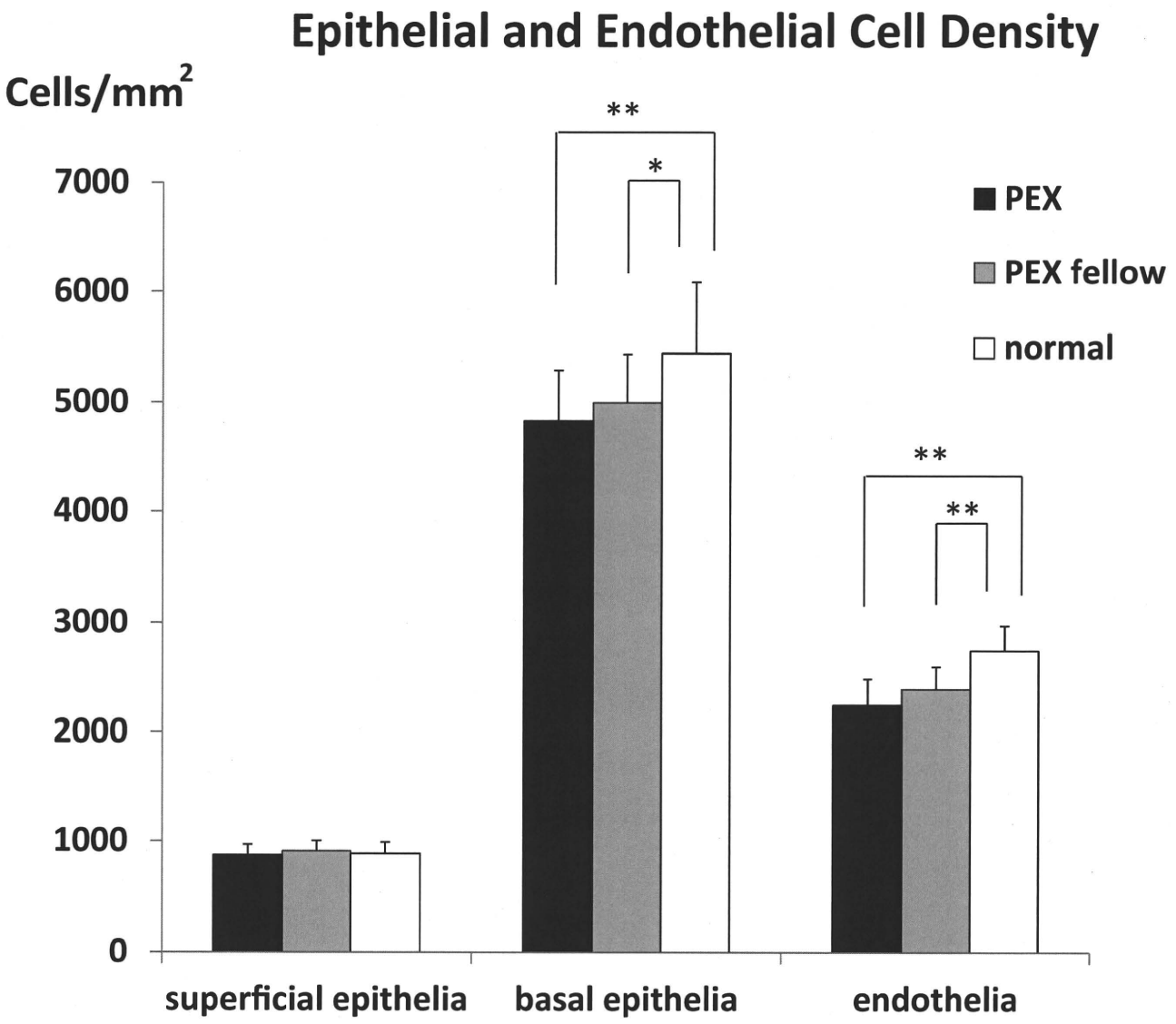
Epithelial and Endothelial Cell Density
Cells/mm2
7000
6000
5000
4000
3000
2000
1000
0
**
*
**
**
PEX
PEX fellow
normal
superficial epithelia
basal epithelia
endothelia

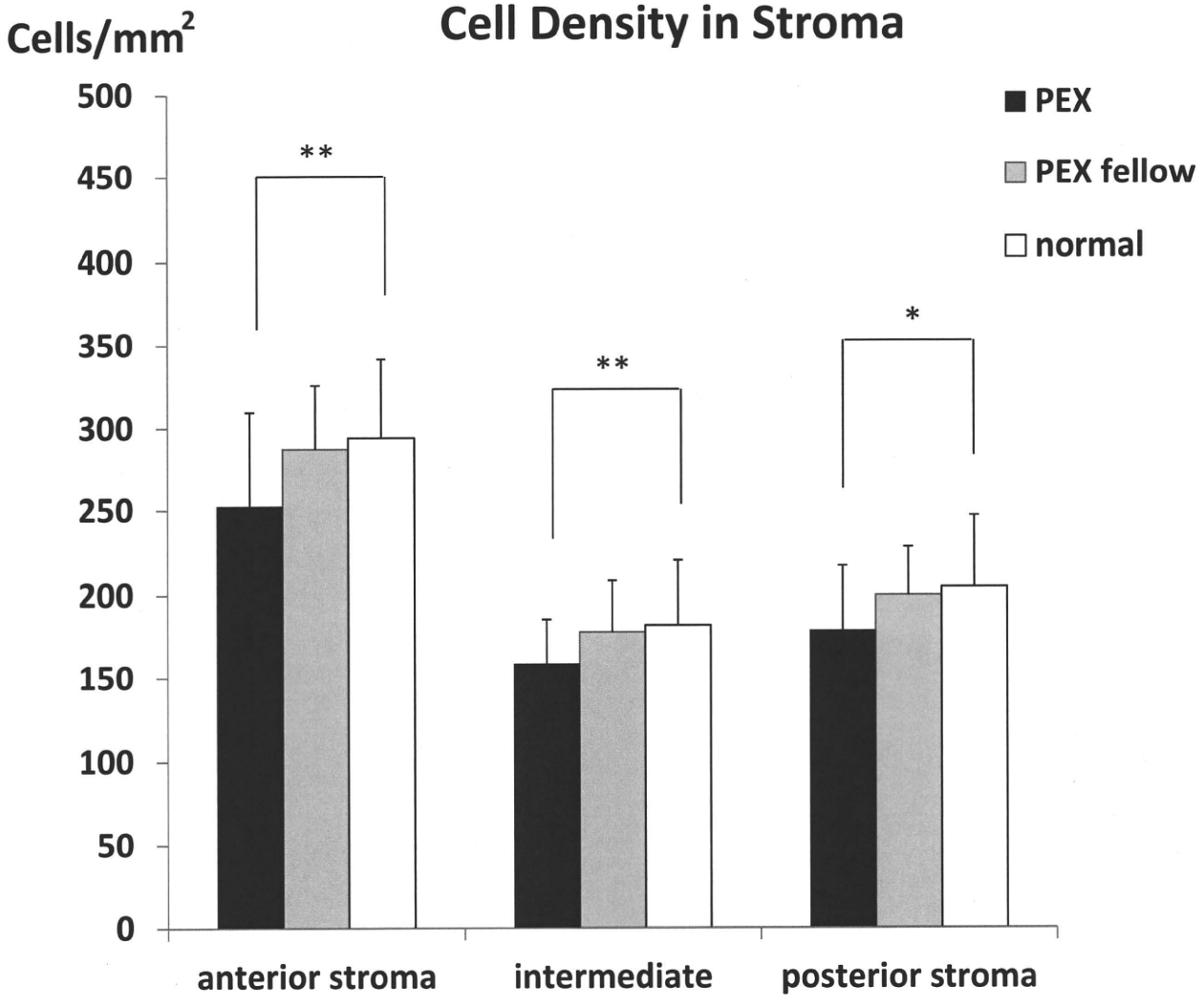
Cells/mm²
Cell Density in Stroma
500
450
400
350
300
250
200
150
100
50
0
**
**
*
PEX
PEX fellow
normal
anterior stroma
intermediate
posterior stroma

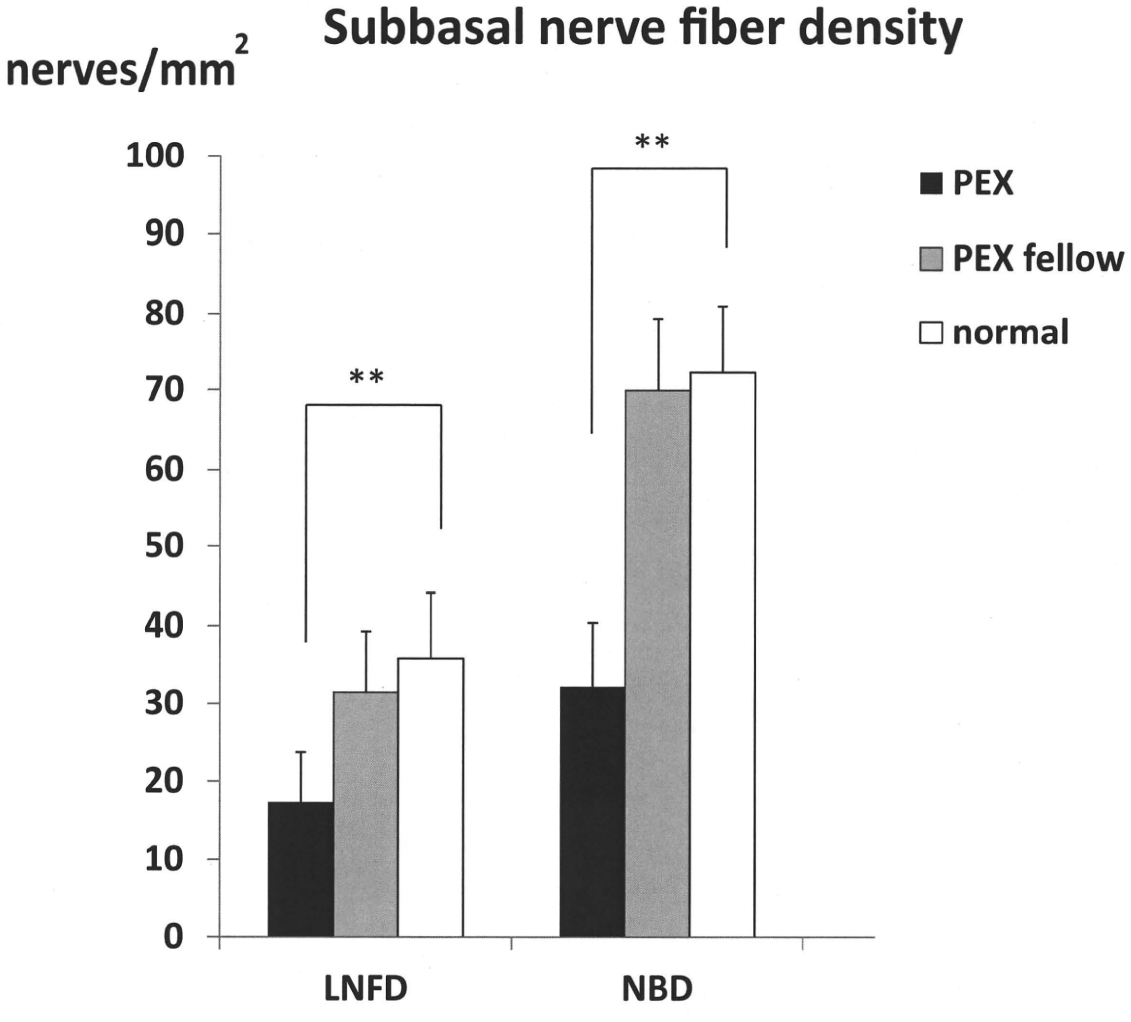
Subbasal nerve fiber density
nerves/mm2
100
90
80
70
60
50
40
30
20
10
0
**
**
LNFD
NBD
PEX
PEX fellow
normal

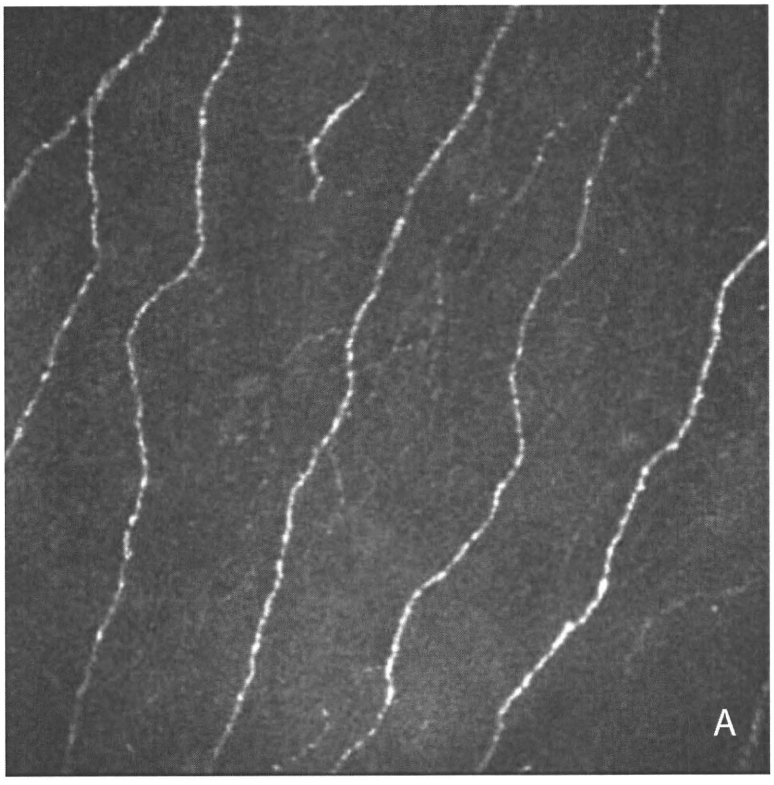
A

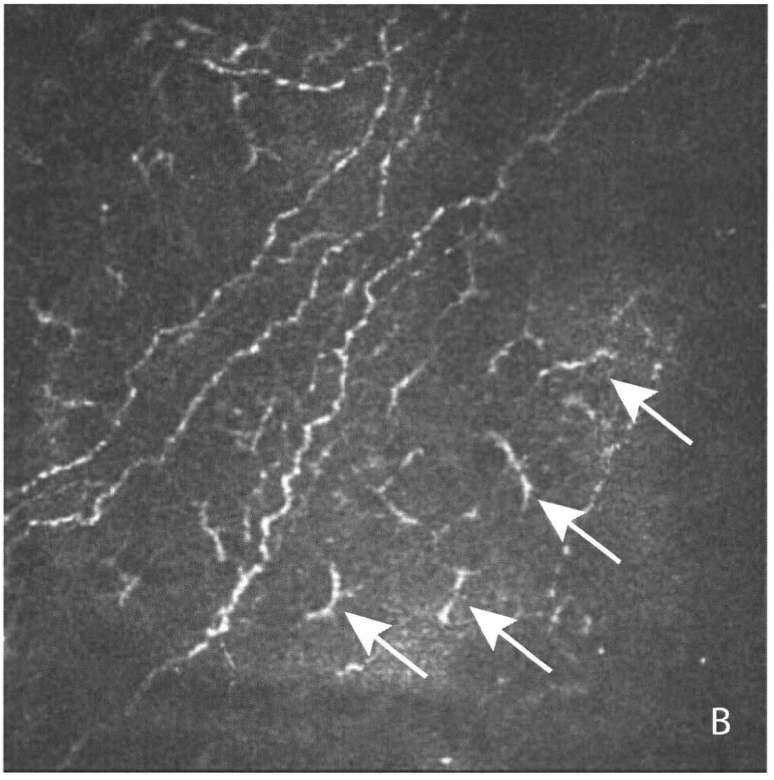
B

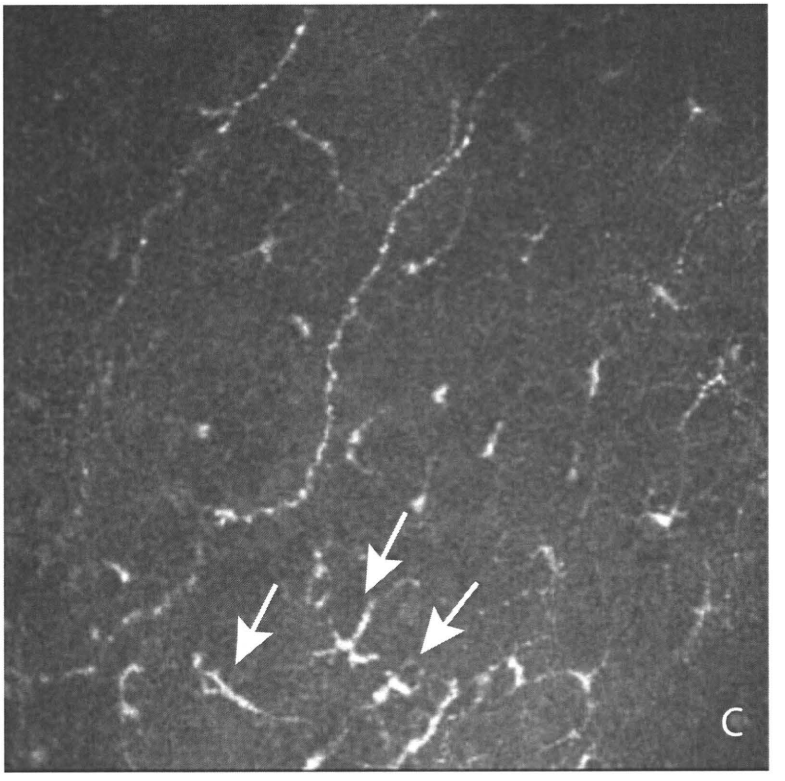
C

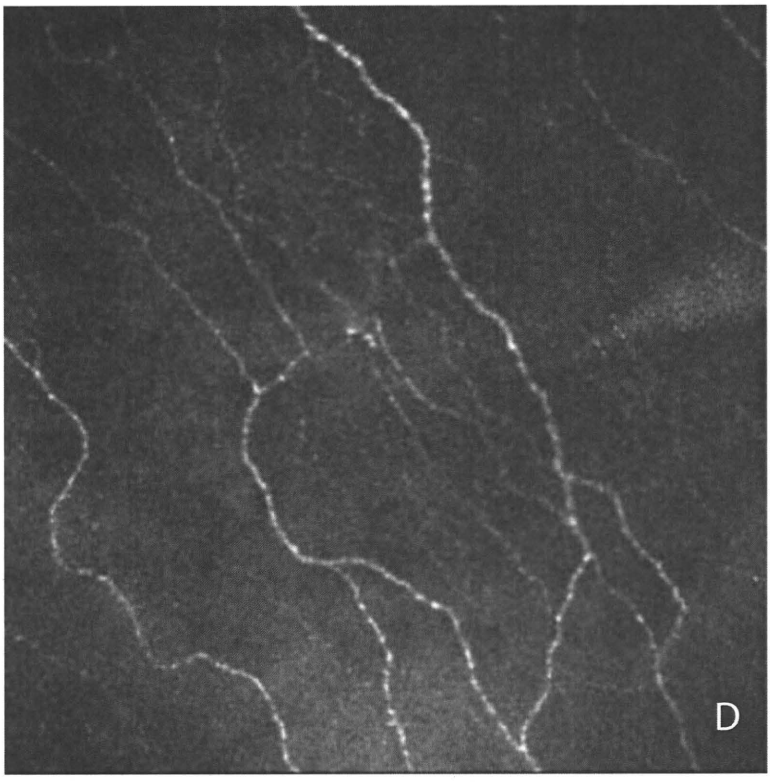
D

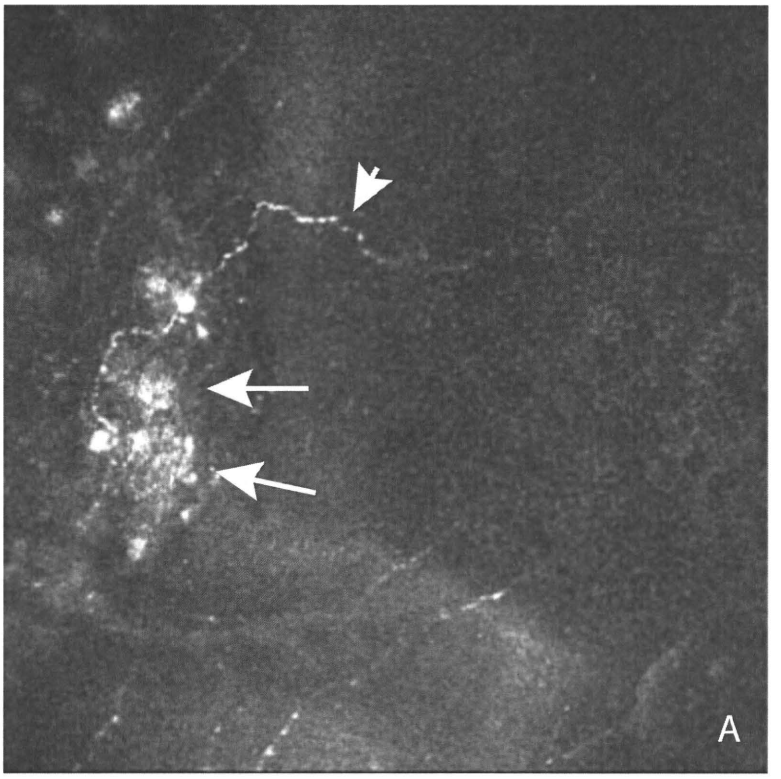
A

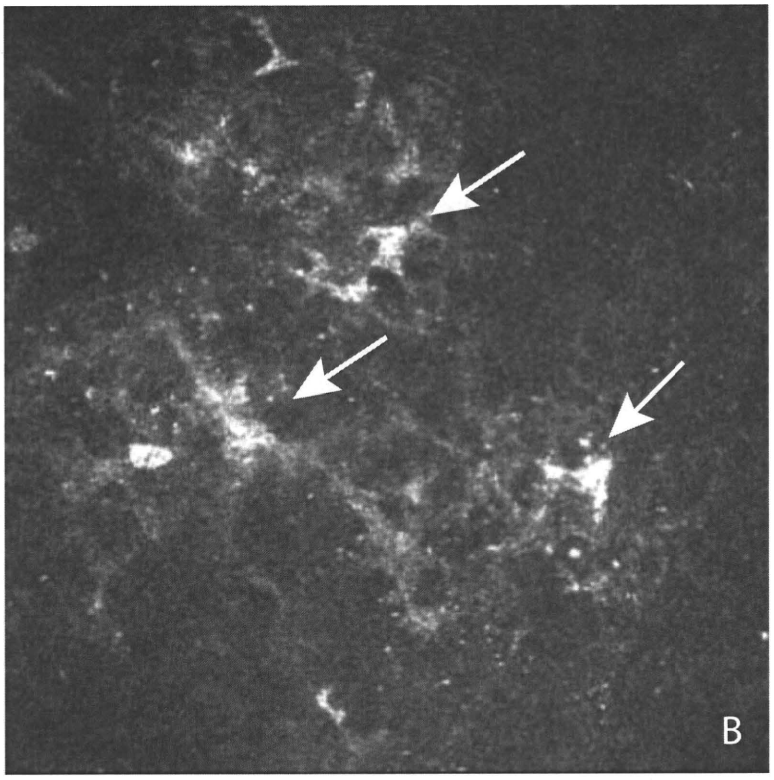
B

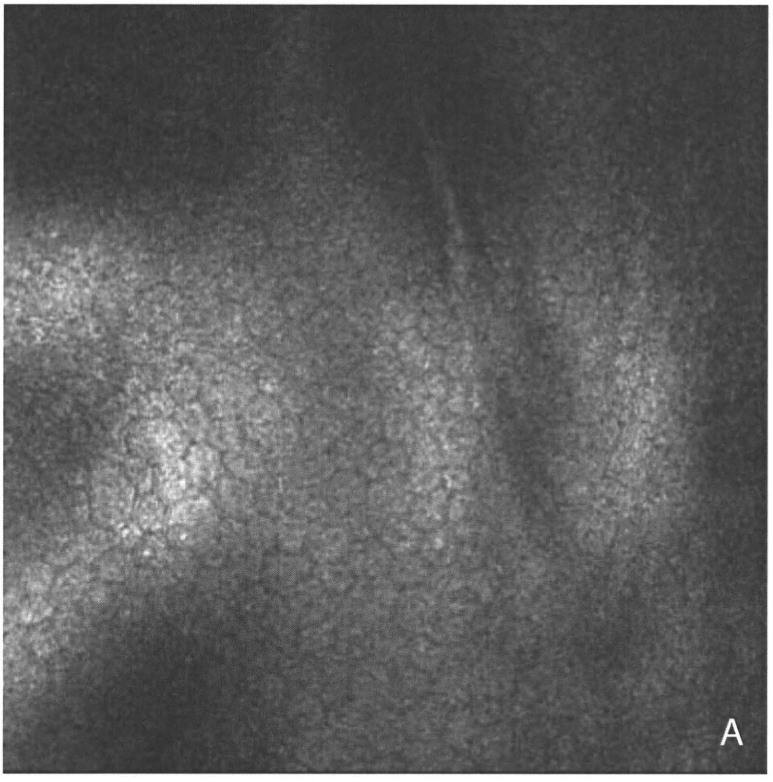
A

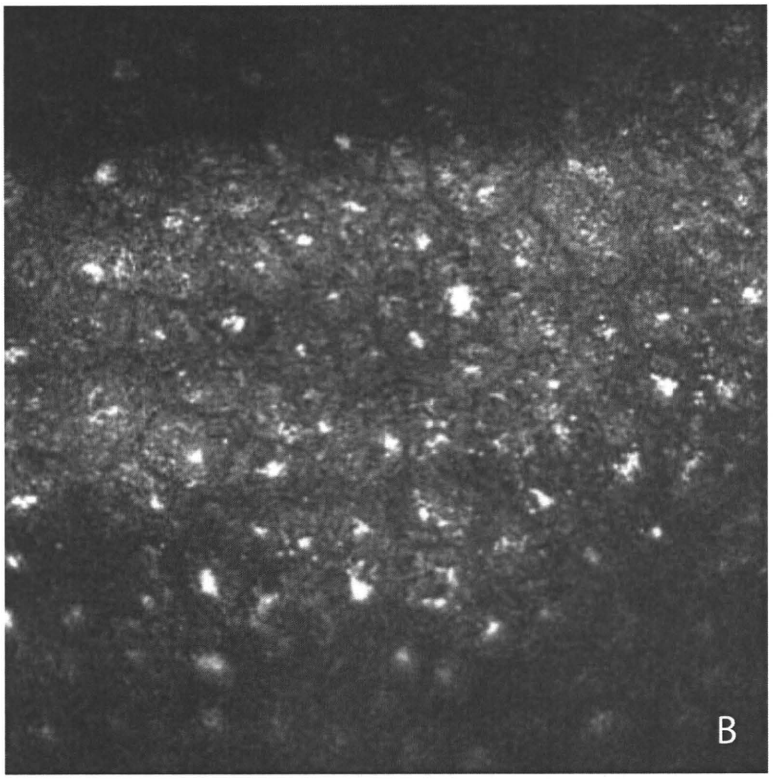
B

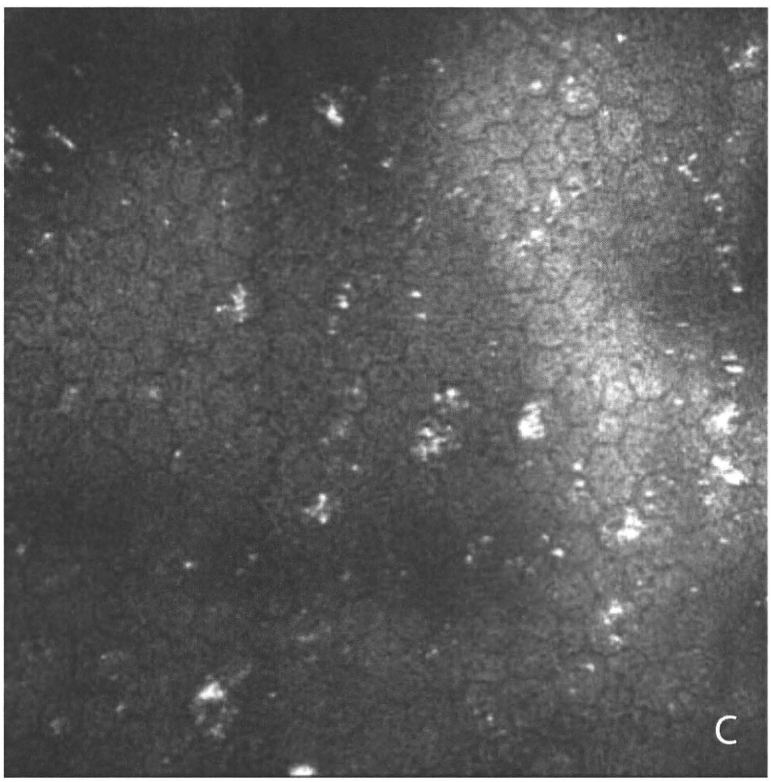
C

Effect of Anterior Chamber Depth on Shear Stress Exerted on Corneal Endothelial Cells by Altered Aqueous Flow after Laser Iridotomy

Yasuaki Yamamoto,[1,2] *Toshihiko Uno,*[1,2] *Takeshi Joko,*[1] *Atsushi Shiraishi,*[1] *and Yuichi Ohashi*[1]

Purpose. The study hypothesis was that shear stress caused by abnormal aqueous flow is one of the causes of corneal endothelial cell loss after laser iridotomy (LI). The shear stress exerted on the corneal endothelial cells (CECs) in anterior chambers (ACs) of different depths was calculated by a computational fluid dynamics program. The effect of shear stress was also examined on human corneal endothelial cells (HCECs) grown on microscope slides.

Methods. Three-dimensional models of the AC were constructed, with and without an LI window, and AC depths of 2.8, 1.8, 1.5, and 1.0 mm. The speed of aqueous streaming through the LI window was obtained from animal studies and used to calculate the shear stress exerted on the CECs. Cultured HCECs attached to glass slides were subjected to different magnitudes of shear stress by exposing the cells to different flow rates of the culture solution. The number of cells remaining attached to the slide under each condition was determined.

Results. The shear stresses were 0.14, 0.31, 0.48, and 0.70 dyn/cm^2 for models with AC depths of 2.8, 1.8, 1.5, and 1.0 mm, respectively. When cultured HCECs were subjected to shear stress within the range calculated by the three-dimensional models, the number of cells remaining attached to the glass slide decreased as the magnitude and duration of the shear stress increased.

Conclusions. Shear stress exerted on CECs after LI may reach a magnitude high enough to cause cell damage and loss in eyes, especially in those with shallow anterior chambers. (*Invest Ophthalmol Vis Sci.* 2010;51:1956-1964) DOI:10.1167/iovs.09-4280

The first case of irreversible corneal edema after argon laser iridotomy (LI) was reported by Pollack[1] in 1984, and five cases of phakic bullous keratopathy after argon LI were reported soon afterward by Schwartz et al.[2] Since then, the incidence of LI-induced bullous keratopathy has increased yearly[1-9] and is now one of the most common reasons for penetrating keratoplasty in Japan.[7-9] Although a variety of hypotheses have been made on the cause of this unique form of bullous keratopathy (e.g., excessive laser irradiation,[2,3,5] an acute glaucoma episode,[2,4] and preexisting corneal endothelial abnormalities such as Fuchs' corneal dystrophy),[2,4,5] many cases cannot be fully explained by these factors. Among these, excessive laser irradiation with subsequent thermal damage of the endothelial cells has been considered to be one of the dominant causes. However, it is puzzling that the corneal endothelial cell density decreases progressively over many years without any significant corneal edema or inflammation immediately after LI.[2-8]

We have demonstrated in animal studies that during miosis, the aqueous humor streams into the anterior chamber (AC) from the posterior chamber through an LI window and strikes the corneal endothelium. During mydriasis, the aqueous humor in the AC is drawn back into the posterior chamber through the LI window.[10]

From these findings, we hypothesized that the shear stress caused by the abnormal aqueous flow striking the corneal endothelium may be one of the pathogenetic mechanisms for progressive corneal endothelial cell loss. To test this hypothesis, we first constructed three-dimensional AC models of different depths, with or without an LI window, and calculated the speed of aqueous flow as well as the shear stress exerted on the corneal endothelium by using a computational fluid dynamics program. We further examined the effect of shear stress on endothelial cells in in vitro experiments. To determine whether the shear stress calculated could have an influence on the corneal endothelium, we exposed human corneal endothelial cells (HCECs) cultured on glass slides to shear stress by exposing them to different flow rates of the culture solution, and examined changes in cell morphology and adhesion.

Methods

Computational Fluid Dynamics

Computational fluid dynamics is one of the techniques of fluid mechanics that uses numerical methods and algorithms to analyze and solve problems that involve fluid flow. A computational fluid dynamics program (Fluent; Ansys Japan K.K., Tokyo, Japan) was used in the study. The finite-volume method was used to solve the Navier-Stokes continuity equations on an arbitrary target flow domain, and appropriate boundary conditions were assigned. The speed of the thermal current was calculated in the geometrical AC models at various AC depths, where the temperature of the posterior corneal surface was set at 36°C and the temperature of the iris surface was set at 37°C. Then, a virtual LI window was created at the 12 o'clock position of the peripheral iris and values obtained from animal experiments were introduced into the model, to calculate the speed of the aqueous streaming through the LI. Changes in the speed of aqueous flow and in the shear stress on the corneal endothelium were calculated in models of different AC depths and streaming from the LI window.

From the [1]Department of Ophthalmology, Ehime University, Ehime, Japan.

[2]Contributed equally to the work and therefore should be considered equivalent authors.

Supported by Grant-in-aid for Innovation 206003 from the Science and Technology Agency of Japan.

Submitted for publication July 7, 2009; revised October 13 and 27, 2009; accepted November 3, 2009.

Disclosure: **Y. Yamamoto**, None; **T. Uno**, None; **T. Joko**, None; **A. Shiraishi**, None; **Y. Ohashi**, None

Corresponding author: Yasuaki Yamamoto, Shitsukawa, Toon, 791-0295 Japan; yyasuaki@m.ehime-u.ac.jp.

Investigative Ophthalmology & Visual Science, April 2010, Vol. 51, No. 4

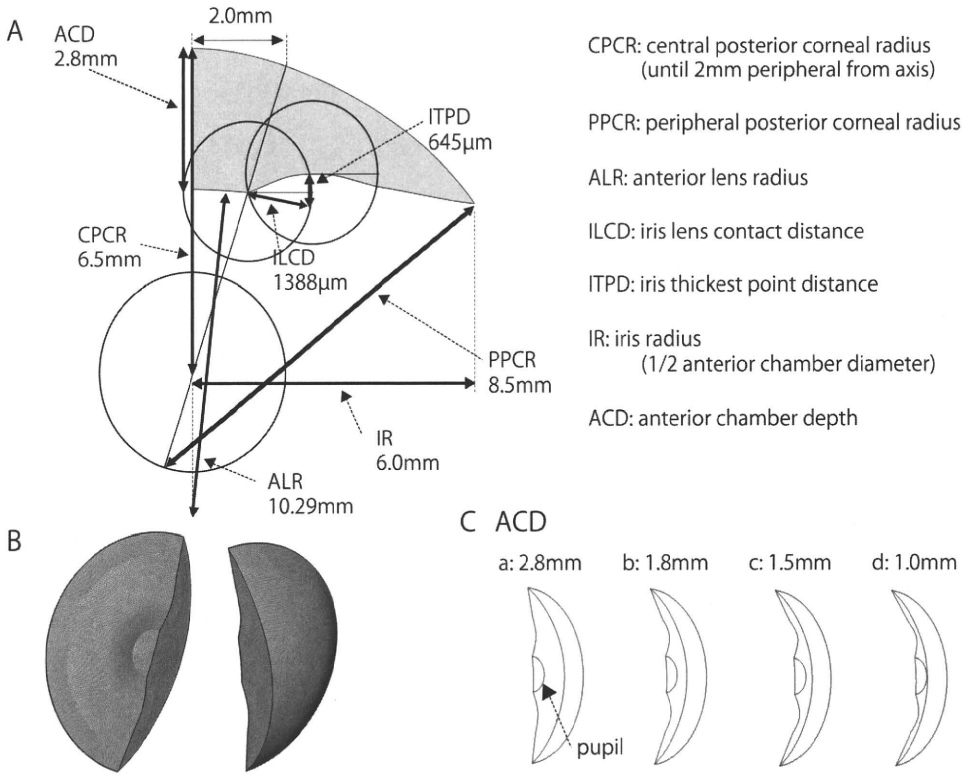

FIGURE 1. Geometric model of the AC of the eye. (**A**) Two-dimensional geometric model of an eye with an AC depth (ACD) of 2.8 mm. The three-dimensional contours were constructed by rotating the two-dimensional shape around the ocular axis. (**B**) Cubic diagram of a divided three-dimensional AC model with a depth of 2.8 mm (adverse side and flip side). In a similar manner, ACs were constructed with ACDs of 1.8, 1.5, and 1.0 mm. (**C**) The outline of divided three-dimensional AC models with a depth of (**Ca**) 2.8, (**Cb**) 1.8, (**Cc**) 1.5, and (**Cd**) 1.0 mm. The half circle outside each model represents the AC angle. The half circle inside each model represents the pupil.

Geometric Model of the AC

Geometric models of the AC were constructed according to the clinical parameters of the AC cited in published reports and by using Bezier curves.[11–13] A two-dimensional AC with a depth of 2.8 mm and its parameters are shown in Figure 1A. A three-dimensional AC with a depth of 2.8 mm was constructed by rotating the two-dimensional shape around the ocular axis. A cubic diagram of a divided three-dimensional AC model with a depth of 2.8 mm (adverse side and flip side) is shown in Figure 1B. In a similar manner, three-dimensional ACs were constructed for AC depths of 1.8, 1.5, and 1.0 mm (Fig. 1C). The 2.8-mm AC depth corresponded to that of a normal eye, 1.8 mm to an eye with a narrow angle, 1.5 mm to an eye with angle-closure glaucoma requiring preventive LI, and 1.0 mm to an eye with an extremely shallow AC during an episode of acute glaucoma requiring LI.

Simulation of Aqueous Streaming in an Eye with an LI Window

We have demonstrated the speed and direction of aqueous flow after LI by particle-tracking velocimetry, using silicone powder as a tracer in rabbit eyes. In that study, the aqueous humor was seen to stream into the AC from the posterior chamber through the LI window during the miosis induced by a light stimulus. The streaming aqueous passed through the LI window beginning at the onset of miosis and continued for the duration of a single miosis as a single pulse, but an aqueous flow through the pupil was not detected. The v_{max} of the forward aqueous streaming through the LI window in eyes with the diameter of the LI window at 0.56 mm was 9.39 mm/s, determined by the particle-tracking velocimetry technique.

From these results, the following parameters were used for the computational fluid dynamics for the study. The diameter of the LI window was set at 0.56 mm, and the position of the LI window was set at the 12 o'clock position of the iris, 1.0 mm away from the AC angle. The initial speed through the LI window was set at 9.39 mm/s. The duration of the analysis time was set to 0.660 second, because that is the average duration of miosis in humans after light stimulation.[14] The attenuation of the speed of aqueous streaming was approximated by a cosine function. Thus, calculations of the speed of aqueous streaming were executed every 0.033 second with the following equation:

$$V(T) = 9.39\cos[\pi T/(2 \times 0.660)]$$

where V is the speed of aqueous streaming (in millimeters per second) and T is time (seconds).

Shear Stress Model Experimental Design

Human corneal endothelial cells (HCECs) were cultured until they reached confluence on a glass slide with a specially designed flow channel. The cells were subjected to various magnitudes of shear stress created by both continuous and intermittent flow of the culture solution. Changes in the morphology of the cells on each slide were observed by optical microscopy after the cells were exposed to shear stress for 4 and 16 hours.

Media and Culture Conditions

All primary and passaged HCECs were cultured in medium consisting of Dulbecco's modified Eagle's medium (DMEM) supplemented with 15% fetal bovine serum, 30 mg/L L-glutamine, 2.5 mg/L amphotericin B (Fungizone; Invitrogen-Gibco, Grand Island, NY), 2.5 mg/L doxycycline (Sigma-Aldrich Co., St. Louis, MO), and 2 μg/mL basic fibroblast growth factor (Invitrogen, Carlsbad, CA).[15] Cultured HCECs were maintained in a humidified incubator at 37°C and 10% CO_2.

Cell Culture Methods

Primary cultures of HCECs were established from normal human corneas obtained from the American Eye Bank. The human tissue was used in strict accordance with the tenets of the Declaration of Helsinki.[16] Primary cultures of HCECs and all subsequent passages were performed by using our published method.[17] We used cultured HCECs at the fifth passage for the experiments.

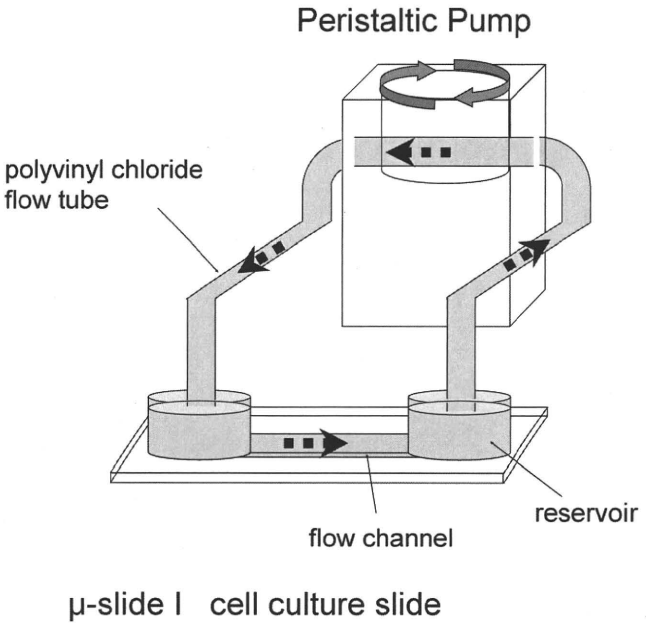

FIGURE 2. Diagram of culture slides and the flow circuit system, a collagen IV-coated cell culture slide, with a flow channel and accompanying flow kit were used. A flow circuit was constructed by connecting a peristaltic pump to a polyvinyl chloride flow tube. HCECs were cultured until they reached confluence on the channel of a glass slide. The cells were subjected to various magnitudes of shear stress created by both continuous and intermittent flow of the culture solution.

Culture Slides and Flow Circuit System

We used a collagen IV-coated cell culture slide, with a flow channel (μ-slide I; Ibidi μ-Slides; Integrated Bio Diagnostics, Munich, Germany) and the accompanying flow kit. The diagram of the flow circuit is shown in Figure 2. The flow was obtained by connecting a peristaltic pump (Minipuls 3; Gilson Inc., Middleton, WI) to a polyvinyl chloride flow tube. A timer system was devised to induce the pump to alternately turn on for 2 seconds and off for 8 seconds, to produce intermittent periods of culture solution flow. In all the flow experiments, cultured HCECs were maintained in a humidified incubator at 37°C and 10% CO_2.

Statistical Analyses

Differences in the number of cells remaining attached to the slide under each magnitude or condition of shear stress were analyzed by ANOVA and the Scheffé multiple comparison test. $P < 0.05$ was considered to be statistically significant.

RESULTS

Speed of Thermal Current for Different AC Depths

The velocities of the thermal current in the ACs for different AC depths are shown in the color-coded maps in Figure 3. Each of the maps shows the inner surface of the AC at the central sagittal plane, and also planes at 2.5, 4, and 5 mm from the center to the nasal and temporal planes. The thermal current flowed down the corneal endothelial surface and up the iris surface. The maximum descending speeds of aqueous flow in the central sagittal plane near the corneal endothelium were 0.23, 0.11, 0.076, and 0.037 mm/s at AC depths of 2.8, 1.8, 1.5, and 1.0 mm, respectively. As the AC became shallower, the speed of the aqueous flow became slower in all planes of the AC examined.

Speed of Aqueous Flow through the LI Window during Miosis

The speed of aqueous flow through the LI window was calculated during a single miosis induced by a light pulse. Figure 4 shows the aqueous flow speeds calculated immediately before the aqueous collided with the corneal endothelial surface opposite the LI window from the onset of miosis (time 0) to the end (time 0.660 second). The measurements were taken every 0.033 second in models with AC depths of 2.8, 1.8, 1.5, and 1.0 mm.

The maximum speeds were 0.84, 1.83, 2.79, and 3.90 mm/s in models with AC depths of 2.8, 1.8, 1.5, and 1.0 mm, respectively. The color-coded maps of the central sagittal plane and the nasal and temporal planes 2.5, 4, and 5 mm from the center (Fig. 4) are the spatial distribution of aqueous flow speeds at the time when flow reached a maximum speed.

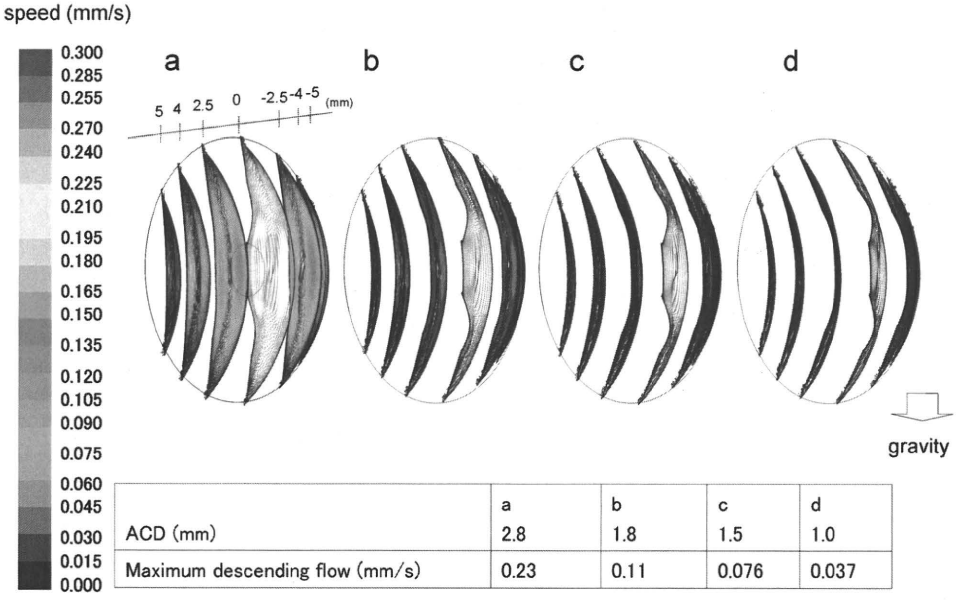

	a	b	c	d
ACD (mm)	2.8	1.8	1.5	1.0
Maximum descending flow (mm/s)	0.23	0.11	0.076	0.037

FIGURE 3. Speed of the thermal current for the different AC depths (ACDs) is shown in the color-coded maps: (**a**) 2.8, (**b**) 1.8, (**c**) 1.5, and (**d**) 1.0 mm. Each color-coded map shows the inner AC in the central sagittal plane and 2.5, 4, and 5 mm from the center to the nasal and temporal plane. The thermal current flowed down the corneal endothelial surface and up the iris surface. Thermal current speeds were slower in eyes with shallower ACDs.

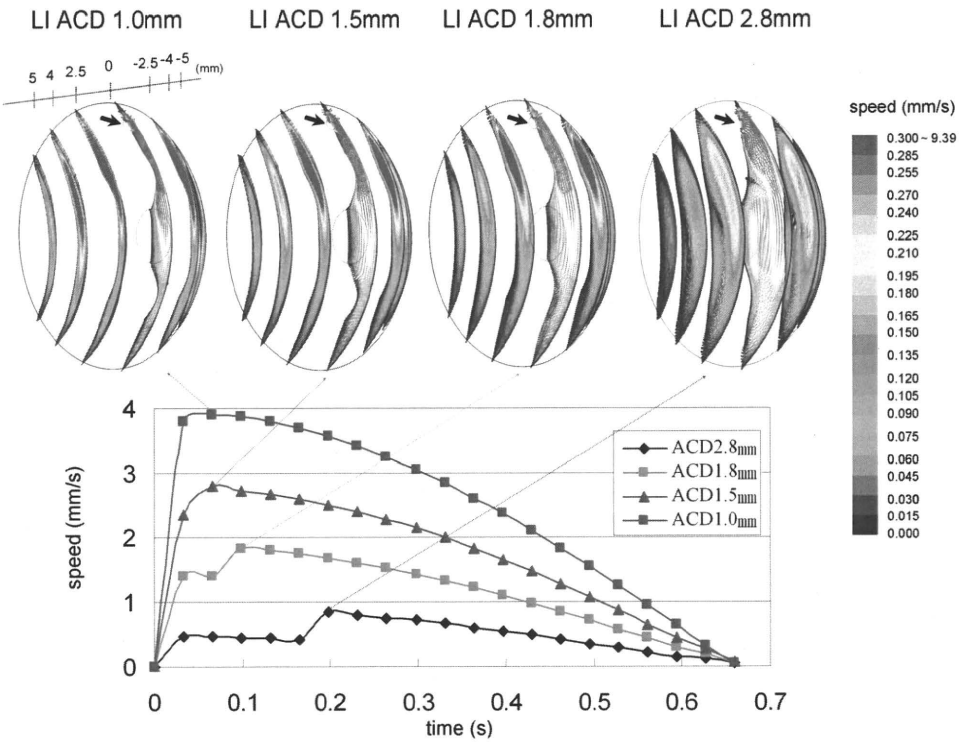

FIGURE 4. The speed of aqueous flow through the LI window was analyzed during a single miosis. The graph shows the aqueous flow speed measured immediately before the aqueous collided with the corneal surface opposite the LI window from the onset (time 0) to the end (time 0.660 second) of miosis. Measurements were taken every 0.033 seconds in models with AC depths (ACDs) of 2.8, 1.8, 1.5, and 1.0 mm. The maximum speeds were 0.84, 1.83, 2.79, and 3.90 mm/s, respectively. Color-coded maps at the central sagittal plane and 2.5, 4, and 5 mm from the center to nasal or temporal plane show the spatial distribution of aqueous flow speeds at the time when flow reached a maximum speed. *Arrows*: the position of the LI window in each AC model.

Shear Stress on Corneal Endothelial Surface in Eyes with an LI Window

The shear stress on the corneal endothelial surface was calculated during the period of aqueous streaming. Figure 5 shows the maximum shear stress exerted on the corneal endothelial surface opposite the LI window from the onset (time 0) to the end (time 0.660 second) of miosis. The values are plotted for every 0.033 second over a 0.660-second period of miosis in models with AC depths of 2.8, 1.8, 1.5, and 1.0 mm, respectively. For each AC depth, the spatial distribution of shear stress on the corneal endothelial surface at the time when shear stress reached a maximum is shown in the color-coded maps (Fig. 5). The maximum shear stresses exerted on the corneal endothelium were 0.14, 0.31, 0.48, and 0.70 dyn/cm^2 for models with AC depths of 2.8, 1.8, 1.5, and 1.0 mm, respectively. For comparison, the shear stress caused by the descending thermal current in a normal eye with an AC depth of 2.8 mm and no LI window, was 0.0062 dyn/cm^2 at the center of the corneal endothelial surface.

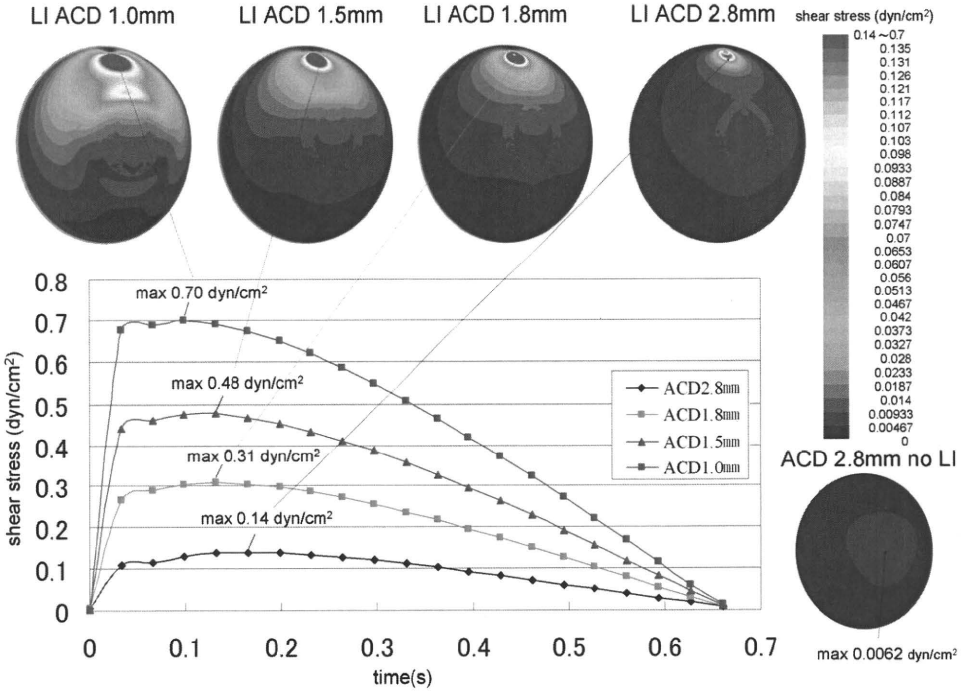

FIGURE 5. The shear stress on the corneal endothelial surface was calculated during the period of aqueous streaming. The graph shows the maximum shear stress exerted on the corneal endothelial surface opposite the LI window from the onset (time 0) to the end (time 0.660) of miosis. The values are plotted for every 0.033 second over a 0.660-second period of miosis in models with ACDs of 2.8, 1.8, 1.5, and 1.0 mm. The maximum values of shear stress exerted on the corneal endothelium were 0.14, 0.31, 0.48, and 0.70 dyn/cm^2, respectively. At each ACD, the spatial distribution of shear stress on the corneal endothelial surface at the time when shear stress reached a maximum is shown in a color-coded map. For comparison, the shear stress caused by the descending thermal current in a normal eye with an ACD of 2.8 mm and no LI window, was 0.0062 dyn/cm^2 at the center of the corneal endothelial surface.